Unraveling the formation mechanism of hybrid Zr conversion coating on advanced high strength stainless steels

Nabizadeh, Mohaddese; Marcoen, Kristof; Amine Mernissi Cherigui, El; kolberg, Thomas; Schatz, Daniel; Terryn, Herman; Hauffman, Tom

Published in:
Surface and Coatings Technology

DOI:
10.1016/j.surfcoat.2022.128567

Publication date:
2022

Document Version:
Submitted manuscript

Unraveling the formation mechanism of hybrid Zr conversion coating on Advanced High Strength Stainless Steels (AHSSS)

Mohaddese Nabizadeh[1], Kristof Marcoen[1] ,El Amine Mernissi Cherigui [2], Thomas Kolberg[3], Daniel Schatz[3], Herman Terryn[1], Tom Hauffman[1]

[1] *Research Group Electrochemical and Surface Engineering, Department of Materials and Chemistry, Vrije Universiteit Brussel, Brussels, Belgium*

[2] *Aperam Stainless Steel, Isbergues, France*

[3]*Chemetall GmbH, Frankfurt, Germany*

1 Abstract

This research unravels the formation mechanism of a hybrid conversion treatment including the well-established Zr conversion coating with a silane-based organic additive and Cu-based inorganic additive. The deposition mechanism of this coating was investigated on the thermal oxide film of Advanced High Strength Stainless Steels (AHSSS). This coating has been characterized using advanced surface analytical techniques such as XPS, FEG-AES, GDOES, and ToF-SIMS. The results showed that the simultaneous presence of these two additives results in the formation of a donor-acceptor complex between amine groups and Cu ions. This can prevent the selective deposition of Zr oxide on Cu-containing zones and result in the formation of a more homogenous coating. The final coating contains Cu oxide together with a Cu-aminosilance complex, Zr oxide deposited mainly around Cu oxide and the aminosilane layer on the outer surface.

Keywords: conversion coating, Tof-SIMS, XPS, Aminosilane, stainless steel

2 Introduction

Advanced high strength stainless steels (AHSSS) have been developed as a compromise for automotive applications to impart both lighter weight and satisfactory mechanical properties to the car body [1–3]. In addition, the optimal amount of Cr content in these alloys provides an excellent level of corrosion resistance [4,5].

During the application of this material in the automotive structure, a stack of coatings is applied on the surface in order to grant various aesthetic and protective properties to the surface [6,7]. In the course of the pretreatment step, as one of the layers, a thin conversion coating is deposited on the metallic substrate by a simple immersion process [8–10]. This coating aims to enhance the adhesion of the next organic layer and also to improve the corrosion resistance of the substrate [11–13]. Following the REACH regulation, the application of chromate and phosphate conversion coatings was restricted due to their health and environmental issues [14,15]. Therefore, numerous research has been conducted to find an environmentally friendly alternative that can provide the same anti-corrosion and adhesion properties.

The investigation in this field showed that the rare-earth-based conversion treatments such as cerium, vanadate, and zirconium-based treatment could be a potential alternative with promising performance [16–18]. Among all these possibilities, Zr-based conversion treatment could become commercialized by exhibiting lower environmental impact and lower operational cost [19–21]. In this type of conversion treatment, the reaction is initiated by the dissolution of the substrate through an anodic reaction [19,22,23]. This reaction leads to hydrogen evolution and oxygen reduction reactions which alkalize the surface of the substrate [23,24]. It is also shown that the coating contains ZrO_2 that is formed during the following reaction [10,20,21,25]:

$$ZrF_6^{2-} + 4H_2O \rightarrow ZrO_2{\cdot}H_2O + 6HF + O^{2-}$$

The more in-depth investigations exhibit that the film formation preferentially occurs on and around intermetallic particles that act as cathodic sites after which then the coating laterally grows [26–28].

Several studies focused on the optimization of coating deposition parameters such as immersion time, pH, and temperature to obtain the best anti-corrosion performance [24,29]. Moreover, the use of inorganic additives in the conversion solution could also help to achieve a better coating in terms of protection and adhesion [30–32]. For instance, Cu is extensively used to increase the deposition rate of the conversion coating [33–36]. Cu particles act as extra cathodic sites and promote the alkalization of the surface which favors the coating deposition [16,37,38]. However, the incorporation of the Cu compound in the solution results in the formation of a non-uniform Zr layer that does not cover the whole surface and this can deteriorate the anti-corrosion behavior of the system [15,31,39].

On the other hand, organic-based conversion coatings such as organosilanes were also introduced as a green alternative to chromate and phosphate conversion coatings [40–42]. These multi-functional molecules can improve the adhesion of paint by having an affinity for both metallic substrate and polymer. They can also form a barrier layer that enhances the corrosion properties [43]. Akhtar et.al showed that 10 min immersion of 304 stainless steel in a silane-based solution could improve the anti-corrosion properties of the substrate [44]. However, the fact that they can only interact with certain paints, as a single component pretreatment, made them less popular in this field [45,46].

Nevertheless, other studies showed the benefit of organic compounds as an additive for the conversion solution in order to achieve an improved base for the subsequent organic layer in terms of adhesion and barrier properties [15,47–49]. These studies led to the idea of a "hybrid-conversion coating" which takes advantage of the combination of both organic and inorganic additives to obtain the optimized properties [15,50,51]. Adhikari et. al studied the corrosion resistance of a steel substrate treated with a Zr-based conversion coating containing a small amount of Si and Cu [15]. They observed that the presence of Cu increased the coating growth rate and led to good long-term corrosion protection. However, they did not provide further information on the formation mechanism. In more recent research by Liu et. al, a new organic-inorganic Zr-based conversion coating containing both Cu and polyamidoamine was studied [50]. They took advantage of a multimodal approach to unravel the effect of these additives in the formation mechanism. They showed that the presence of the organic additive limits the typical role of Cu and by doing so provides better corrosion protection and adhesion performance. It was suggested that the organic additive controls the free Cu^{2+} via complexation and this results in more optimal properties. However, they could not show the exact chemical composition of this complex.

In this study, the formation mechanism of a hybrid conversion coating based on the combination of hexafluorozirconic acid and aminosilane (Zr-AS) with the addition of Cu^{2+} ions on AHSSS will be investigated. The main goal here is to understand the role of the simultaneous presence of Cu and aminosilane in the deposition mechanism of this Zr-based coating. In this regard, a multi-analytical approach was employed. The blank and treated samples were characterized using Scanning Electron Microscopy (SEM), Energy Dispersive X-ray spectroscopy (EDX), and Field Emission Gun Auger Electron Spectroscopy (FEG-AES). In addition, the surface and the in-depth (molecular) composition of the samples were examined by means of Time-of-Flight Secondary Ion Mass Spectrometry (ToF-SIMS) and Glow-Discharge Optical Emission Spectroscopy (GDOES) to obtain a comprehensive understanding of the conversion treatment through depth. High-Angle Annular Dark Field Scanning Transmission Electron Microscopy (HAADF-STEM) was also employed to observe composition of the cross section of the sample before and after treatment.

3 Experimental and methods

3.1 Materials and treatments

In this study, Advanced High Strength Stainless Steel (AHSSS) from Aperam Stainless Steel was used as a substrate. The chemical composition of this substrate was measured by Wavelength Dispersive X-ray Fluorescence spectrometer (WDXRF) that is mentioned in our previous research [3]. This material contains 11 wt.% Cr and less than 1 wt.% of Ni, Mn, Si, and Nb. Additionally, the martensitic structure was obtained after heat treatment of this material at 950° C for 5 min and then colling down in the air.

Prior to the application of hybrid Zr-aminosilane conversion coating, the cleaning step was performed in a commercial alkaline solution (pH 10.5, 10 min, and 55° C) to remove the contamination and prepare the substrate for the conversion process. After the cleaning step, the substrate was immersed in the conversion coating solution based on H_2ZrF_6, Cu nitride, and aminosilane for 3 min at 35° C. In addition,

the fluoride content was kept at 35 ppm for all the sample preparations. Before any analysis of the samples, they were dried in an industrial oven at a temperature of 80°C for 15 min.

3.2 Analysis methods

The characterization of the treated sample by hybrid Zr-AS conversion coating was done using various surface analytical techniques. These techniques were chosen in a way to obtain the maximum information about the structure of the coating and its formation mechanism.

In this regard, Scanning Electron Microscopy (SEM) and Energy Dispersive X-ray spectroscopy (EDX) were utilized in order to evaluate the morphology and elemental composition of the surface, respectively. Moreover, a measurement by glow discharge optical emission spectroscopy (GDOES) was performed to determine the precise variation of chemical composition in the depth of the conversion coating.

The high resolution measurement by X-ray Photoelectron Spectroscopy (XPS) and the Time-of-Flight Secondary Ion Mass Spectroscopy (Tof-SIMS) were performed to determine the oxidation state of different elements and detailed chemical composition of the coating on the surface and at the depth with higher depth resolution. Additionally, The cross-section of the samples was characterized by High-Angle Annular Dark-Field Scanning Transmission Electron Microscopy (HAADF-STEM).

The experimental conditions of the abovementioned measurements were fully explained in our previously published papers [3,4].

Furthermore, the combination of high lateral and depth resolution was achieved by using a Field Emission Gun Auger Electron Spectroscopy (FEG-AES) from JEOL (JAMP-9500F). The image was obtained using a secondary and a backscattered electron detector attached to the FE-AES system at a magnification of ×20000 using a beam of 10 keV and 25 nA. The angle of incidence was 30° with respect to the sample surface. The data were processed using the JEOL Image and Spectra Investigator software.

4 Results and discussion

4.1 The morphology and the chemical composition after the application of hybrid Zr-aminosilane (Zr-AS) conversion coating

Fig. 1 shows the SEM images of the coating on the surface before and after conversion coating. Fig. 1a shows the initial state of the surface (blank sample) containing a fine oxide structure. Fig. 1b shows the surface of the oxide film after treatment with Zr-based conversion coating combined with aminosilane (Zr-AS) with Cu. In this sample, the deposition of scattered particles all over the surface can be observed. To determine the chemical composition of these particles, EDX measurement (Fig. 1c) was performed on one of the particles (marked yellow) and a zone where there is no particle (marked red). The comparison of these two spectra indicates that these particles have a higher concentration of Cu compared to the rest of the surface.

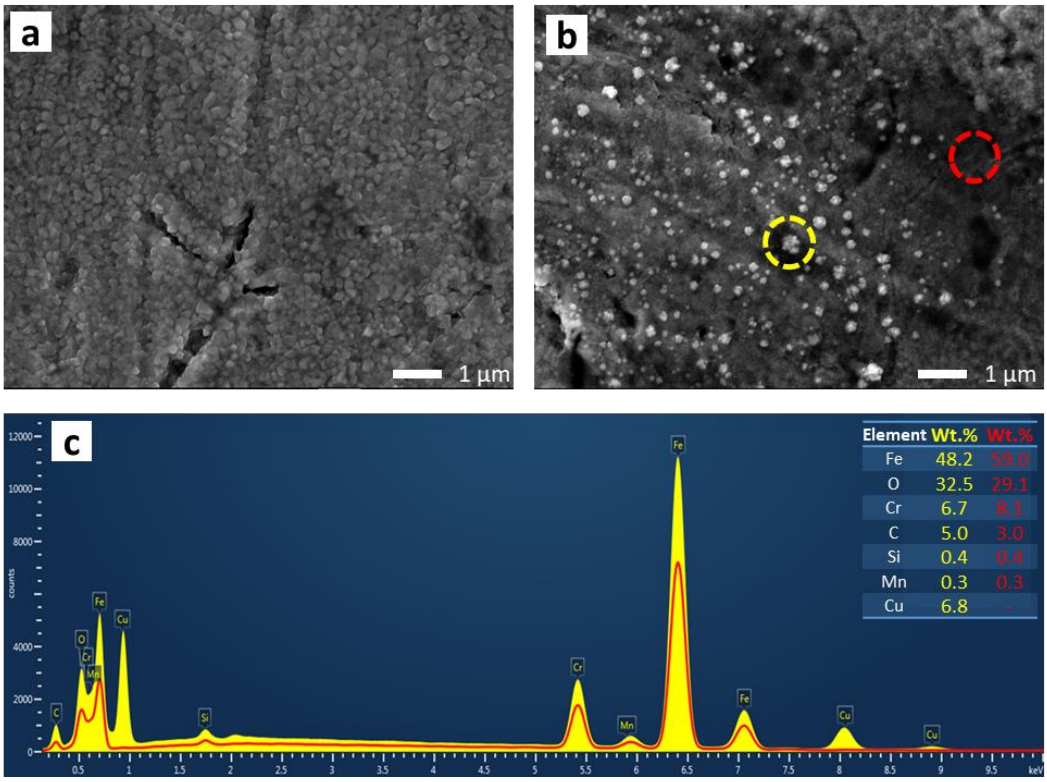

Fig. 1: The SEM images of the surface before (a) and after the application of conversion treatment (b).

c) The EDX spectra of marked zones on Fig. 1(b)

EDX mapping was also carried out in order to extend the understanding from EDX point measurements to the whole surface. Fig. 2(a,b) shows an area of the surface with the corresponding EDX map. Fig. 2b shows that these particles are scattered all over the surface and they mainly consist of Cu.

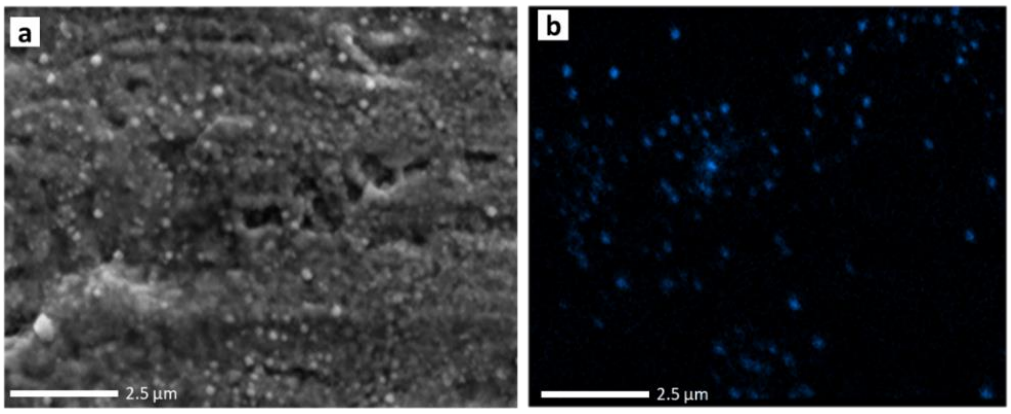

Fig. 2: The SEM image of the treated sample (a) and the corresponding Cu EDX map (b)

4.2 The depth profile after the application of hybrid Zr-aminosilane (Zr-AS) conversion coating

The depth analysis of the blank and treated sample was performed using Glow-Discharge Optical Emission Spectroscopy (GDOES). These measurements were carried out to determine the precise variation of

different elements along the depth and particularly on the top surface. Fig. 3a shows the depth profile of Fe, Cr, Si, and O of the blank sample. The blank sample contains a thermal oxide layer on the top as was explained in the experimental part. We reach the substrate after almost 3s of sputtering, characterized by constant intensities of Fe and Cr. Consequently, the depth profile up to 3s of sputtering shows the variation of composition along the thermal oxide film. The outer layer of the oxide layer is covered mainly by Fe oxide (point number 1) until it reaches the Cr-enriched layer at 2s of sputtering (point number 2). This is followed by a Si-rich zone at 2.5s sputtering time (point number 3). The comprehensive characterization of the oxide layer has been published in our previous research [3]. Fig. 3(b,c) depicts the depth profile of the Zr-AS treated sample in the presence of Cu. The comparison of the O intensity on the top surface (until 0.5s of sputtering) in blank and treated samples clearly shows that the amount of O increased on the very top surface after treatment. This indicates that these treatments resulted in the formation of an oxide/hydroxide on the outer surface. The enlarged depth profile of the top surface of the treated sample in the presence of Cu has been shown in Fig. 3c. This graph shows the presence of two zones where each of the contributing elements in the coating reaches its highest intensity. The first zone on the outermost surface shows the presence of N and Si as an indication for the deposition of aminosilane. At the same zone, Cu can be also observed together with N and Si. In the second zone, Cu reaches its maximum intensity where Zr is also detected. This zone is extended until almost 1 s of sputtering and expands until the enrichment of Cr. These results show that the deposition of Zr happens faster than aminosilane deposition since this element was detected in the lower layer. Also Cu is present throughout the conversion layer.

4.3 Determination of the Cu role on the distribution of Zr-AS coating on the surface

A point by point analysis of the surface was performed using Field Emission Gun Auger Electron Spectroscopy (FEG-AES), to determine the distribution of Zr-AS coating over the surface and particularly around Cu particles. Fig. 4a shows the measurement area for the spot and line measurements by FEG-AES. This figure exhibits surface morphology similar to what has been observed in Fig. 1c in lower magnification. Fig. 4b presents the Auger spectra for the two representative spots on Fig. 4a which are highlighted in red and green. The green spectrum that corresponds to the green-marked particle shows the presence of mainly Cu and Zr. The presence of Cu at these scattered particles was previously observed in Fig. 2b. However, Zr was not possible to be detected by EDX due to its lower surface sensitivity compared to FEG-AES. On the other hand, the red spectrum that corresponds to the red-marked particle indicates the presence of Cu and N and a lower Zr concentration. This deposition pattern has been observed all over the surface of different samples. This shows the competitive deposition of N and Zr on the Cu particles.

In addition to the spot measurements, a line profile of the surface (red line in Fig. 4a) was recorded using FEG-AES as shown in Fig. 4c. The blue line profile indicates the Cu-containing spots along the line. Following the variation of the Zr line profile (in red) clearly shows the enhanced deposition of Zr on or around Cu particles. The line profile of N (in green) does not show a clear trend along the line similar to what has been observed in the spot measurement. This can be due to the low intensity of the N peak.

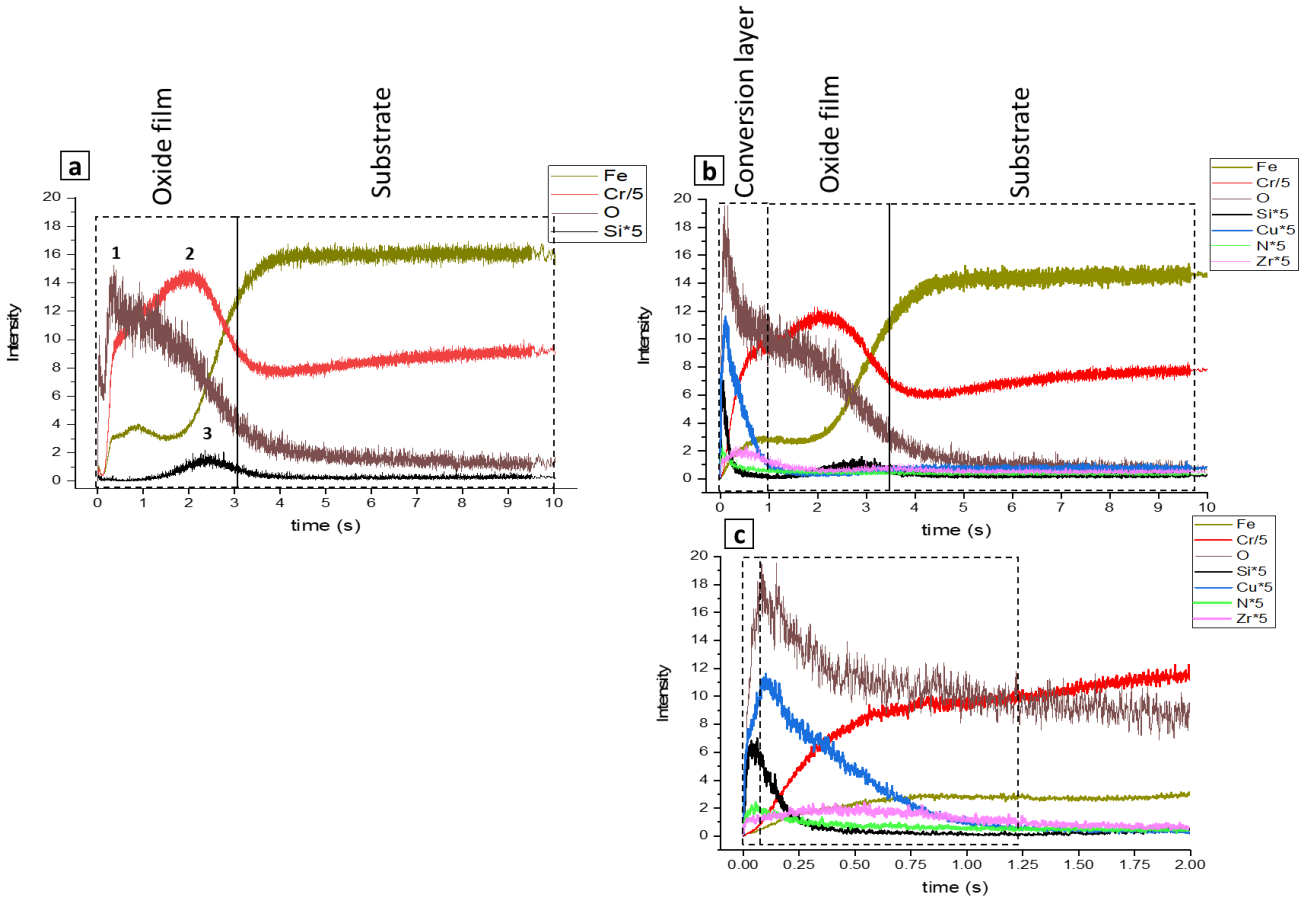

Fig. 3: The GDOES depth profiles of the blank sample (a), the conversion treated sample (b) and its magnified profile until 2 s of sputtering (c)

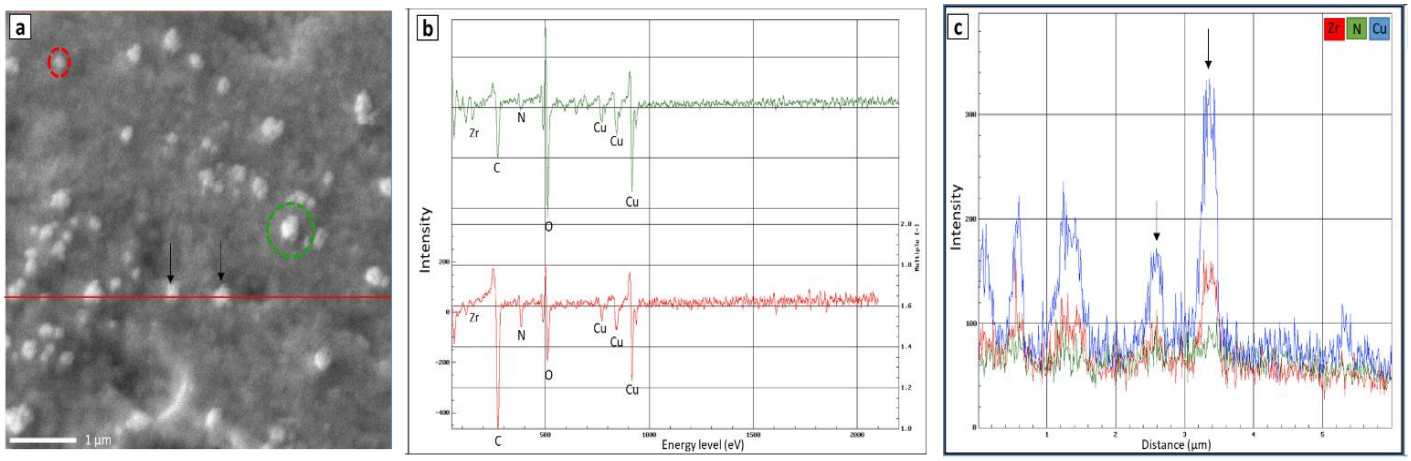

Fig. 4: The SEM image of the treated sample (a), the differentiated FEG-AES spectra of two marked spots on (a) and the FEG-AES line profiles of Cu, Zr, and N (c) corresponding to the red line on (a). The black arrows on (a) and (c) show the correlated spots in the image and the line profile.

4.4 Determination of the Cu and N chemical state on the surface

Determination of the chemical state of Cu is an important tool to understand the mechanism of conversion treatment on this substrate. As reported in the literature [31,33], the Cu^{2+} ions in the solution can be reduced and deposited on the surface as metallic Cu. It is also suggested that the deposited metallic Cu can be oxidized in contact with air or the solution [28,50]. Therefore, it is of importance to figure out the chemical state of Cu in this process to gain a better understanding of the governing mechanism. In this regard, X-ray Photoelectron Spectroscopy (XPS) has been used to determine the oxidation state of the Cu particles. Fig. 5(a-d) demonstrates the high resolution spectra of the Cu2p and Cu LMM peaks on the top surface and after a short period of sputtering, respectively. Fig. 5a shows the Cu2p high resolution spectra on the surface. It indicates the presence of three components in the $Cu2p_{1/2}$ peak at the binding energy of 932.1 (±0.1), 933.3 (±0.1), and 934.8 (±0.2) eV with full width at half-maximum (fwhm) of 1.6 (±0.2) eV. The first component at 932.4 eV corresponds to Cu(0) or Cu(I) [52,53]. Fig. 5b shows the location of the Cu LMM peak of the surface at the kinetic energy of 912 eV. This can show that the first component at 932.4 eV can be assigned to Cu(I) which can be present in the form of Cu_2O and CuOH [54]. The assignment of the third component can also be done according to the binding energy and presence of the shake-up peak between 940 and 945 eV which shows the formation of Cu(II). This peak shows the presence of $Cu(OH)_2$ on the top surface. The second peak located around 933 eV represents the coordination of Cu ions with a group of atoms that are less electronegative than 2 OH groups. Thus, the XPS peak would appear in the lower binding energy than 934 eV. The tendency of the coordination of Cu with N from the amine group has been mentioned in several reports [50,55–58]. In fact, the amine-containing compound has been historically used in order to extract Cu ions from waste water [59–61]. It is reported that Cu(II) can coordinate well with the N in the amine group to form a donor-acceptor complex [55,61]. Therefore, the peak at the binding energy of 933.3 eV can be assigned to Cu-AS as a product of charge transfer between the N in the aminosilane molecule and Cu ions. However, this peak disappeared after short sputtering, indicative for the formation of a very thin layer.

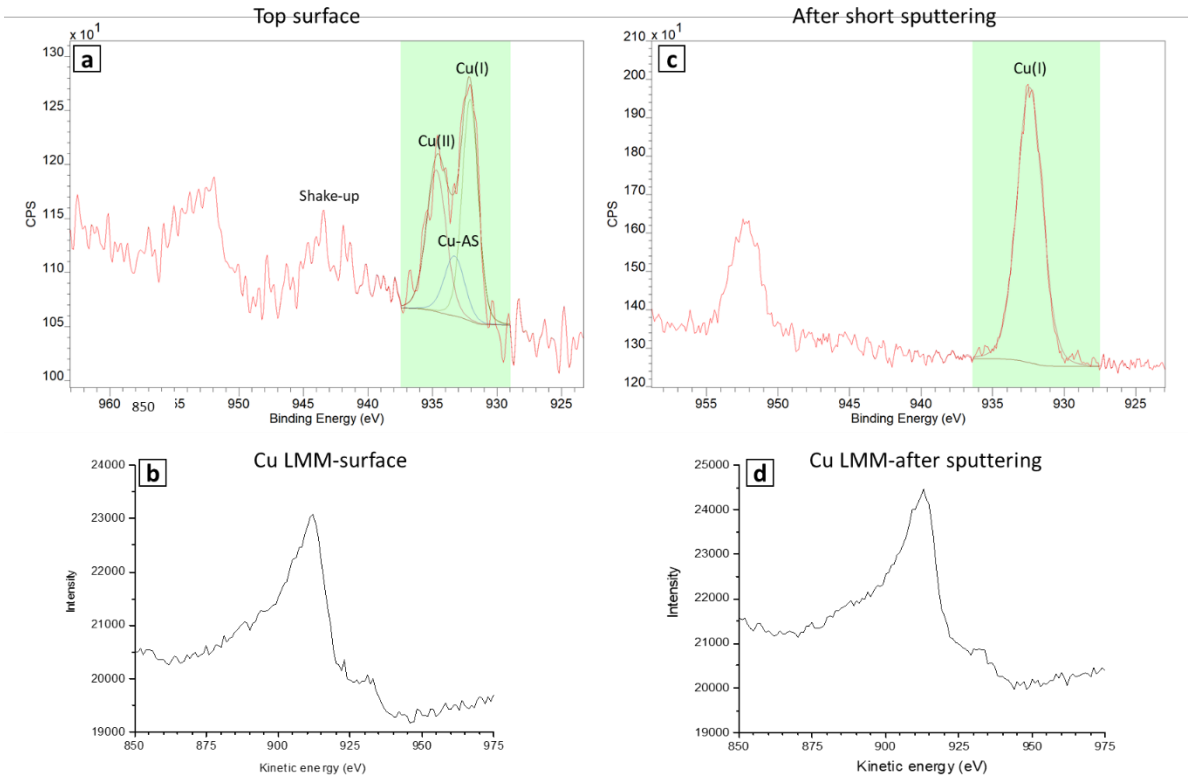

Fig. 5: The high resolution spectra of Cu2p and Cu LMM peak on the top surface (a,b) and after a short sputtering (5s) by Ar^+ ion (c,d)

According to Fig. 5c, the $Cu2p_{1/2}$ peak after a short sputtering (5s) by Ar^+ ion shows only the presence of one component at 932.4 (±0.2) eV (fwhm=1.6 (±0.2) eV). By looking at the Cu LMM peak of the sample after sputtering (Fig. 5d), it can be stated that this peak is located at the kinetic energy of 913 eV which shows the same composition as the first peak in the sample before sputtering, namely Cu (I) [52,54]. Plus, there is no shake-up peak observed that can verify the absence of Cu(II). In addition, Fig. 1S in the supplementary data shows that the deposited Cu in this study has a fully oxidized structure and no metallic Cu was observed in the inner layer.

In conclusion, it can be stated that the Cu(II) component is only present on the top surface and the Cu(I) component is present on the top surface and/or in the inner layer forming a core-shell structure.

Fig. 6 presents the high resolution spectra of N1s on the top surface comprising of two components. The first component (N1) at a binding energy of 400.2 (±0.2) eV corresponds to reported values for Lewis acid−base interaction and is associated with the hydrogen interaction of the amine group with the surface hydroxyl group or the unbound N [62,63]. The second component (N2) at the binding energy of 402.2 (±0.2) eV indicates a higher shift in the binding energy that can be attributed to a high electron density of protonated N in the form Cu-AS [55,64,65]. This component indicates that the N atoms donate their electron pair into a vacant orbital forming a donner-acceptor complex [66,67]. This confirms the previous statement about the possibility of Cu-AS formation.

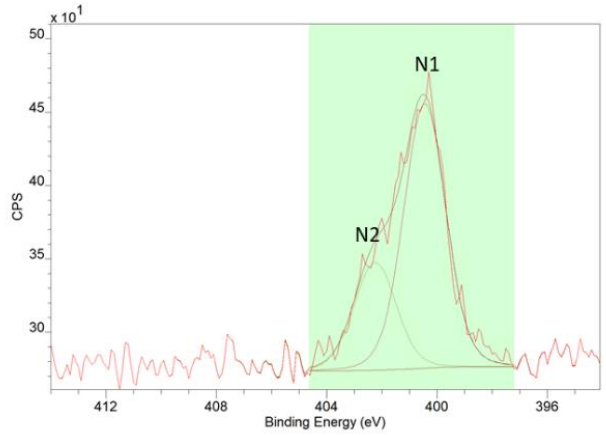

Fig. 6: The high resolution spectra of N1s on the top surface

4.5 The supplementary depth and surface characterization of the Zr-AS treated sample by ToF-SIMS

Time-of-Flight Secondary Ion Mass Spectrometry (ToF-SIMS) was exploited in order to investigate the detailed chemical structure of the sample at the surface and in depth. In this regard, a step-by-step sputtering and measurement characterization was carried out to unravel the depth composition and the mechanism of this process. Fig. 7 presents the signal intensity of $^{65}Cu^+$, ZrO^+, CH_4N^+, and $SiO_3H_3^+$ on the top surface and at 10 nm and 100 nm depth. These four fragments represent three key components of the coating; Cu, Zr, and aminosilane. A spectrum obtained on a sample treated in the absence of Cu is also shown in the overlay (in blue color) to accentuate the role of Cu.
Cu^+ is present throughout the depth and is found with the highest intensity at the depth of 10 nm. ZrO^+ indicates that Zr from the solution has been deposited as Zr-oxide which was previously reported [17,20]. The comparison of ZrO deposition in the absence and presence of Cu shows that Cu has a significant influence on the deposition of ZrO. ZrO^+ is most intense at 10 nm depth. The similar variation of intensities of ZrO^+ and Cu^+ throughout the depth shows that the deposition of ZrO has a direct relation with Cu deposition: more Cu leads to more ZrO deposited.

$CH_4N^+$and $SiO_3H_3^+$ are representative for the deposition of aminosilane on the stainless steel [68]. It can be seen that these two fragments are most intense at the top surface. This result shows again that the deposition of Zr happens faster than aminosilane deposition.

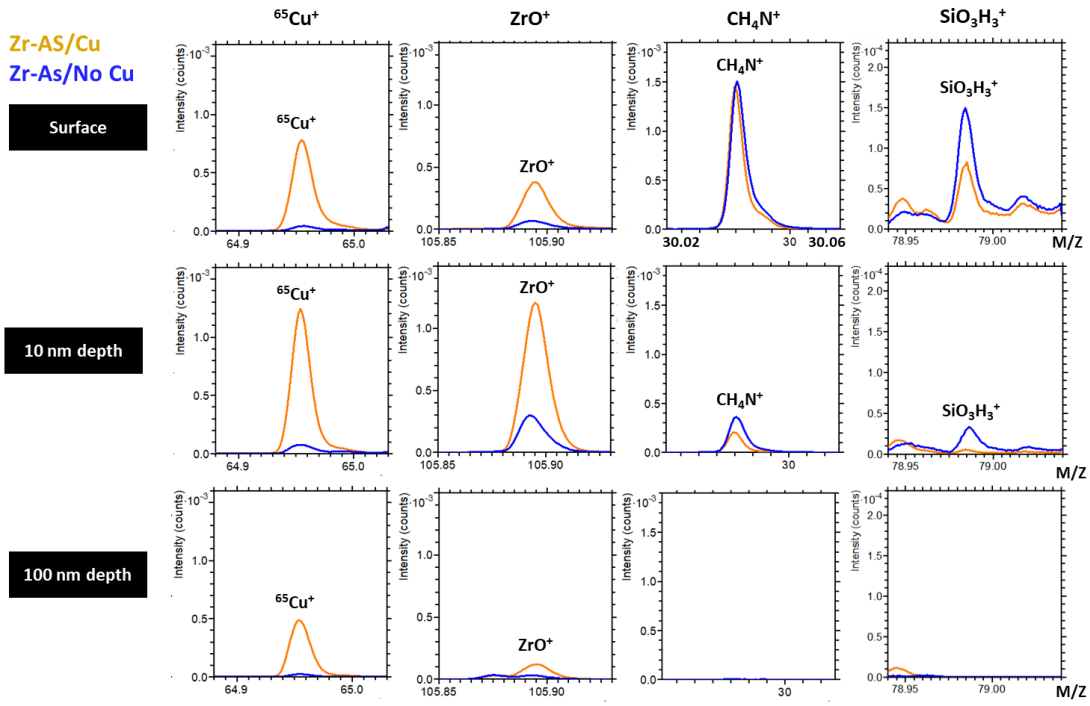

Fig. 7: The comparison of the ToF-SIMS depth profile for different fragments at different depths

It was previously observed in section 4.4 that Cu can be present in different chemical compositions. Therefore, ToF-SIMS analysis was used to identify the different chemical compositions of Cu. Fig. 8 shows the presence of different Cu-containing fragments on the surface and at 10 and 100 nm depth. Cu seems to be present in the form of Cu-oxide/hydroxide (Cu_2O^+, CuO_2^-, and $CuOH^+$), and also it can form some complexes with the substrate itself ($CrCuO^+$ and $CuFeO^+$). Additionally, $CuNH_3^+$ was found in this sample.

It can be seen that Cu_2O^+, $CuOH^+$, and $CuNH_3^+$ are mainly present in the top layer, and that there is no trace of them at 100 nm depth. On the other hand, CuO_2^-, $CrCuO^+$, and $CuFeO^+$ are most intense at 100 nm depth.

The complexation of Cu with Fe-oxide and Cr-oxide from the substrate indicates that the Fe and Cr-oxides could be dissolved and interact with the Cu ions during the conversion process. It can be also stated that the formation of CuO_2^- fragment can show the interaction of Cu ions with the oxide. Nevertheless, the formation of $Cu_2O^+$and $CuOH^+$ mainly on the top surface shows the interaction of the Cu ions with the oxygen or moisture in the solution.

In addition, the observation of $CuNH_3^+$ on the top surface indicates the interaction of Cu ions with the amine group of aminosilane as also seen the XPS measurements.

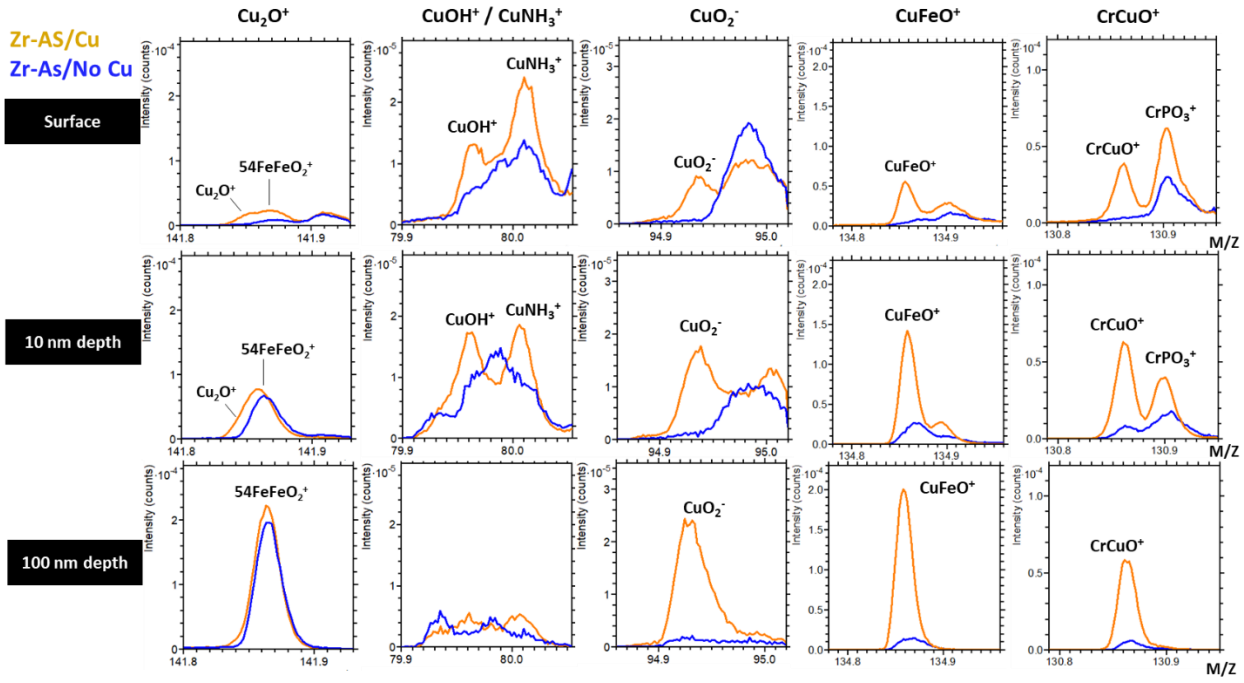

Fig. 8: The comparison of the ToF-SIMS depth profile for different Cu-containing fragments at different depths (The peak of $54FeFeO_2^+$ was indicated to consider the overlap of this fragment with Cu_2O^+)

Fig. 9a shows the signal intensity of $^{65}Cu^+$ on the top surface and at different depths towards the substrate. It can be observed that up to a depht of 200 nm. Cu is no longer detected at a depth beyond 300 nm where the substrate is reached.

HAADF-STEM imaging was performed to verify the presence of Cu in the depth of the oxide layer and also to determine the zones of the oxide layer that this fragment is located. Fig. 8b displays the HAADF-STEM image of an area of the surface containing Cu particle together with the EDX maps of Si, Cu, and Cr.

This observation also verifies that Cu is present in the deeper regions of the oxide layer. The EDX map of Cu shows that this element can be present both as a particle on the top surface and a partial layer in the deeper area of the oxide film. According to these EDX maps, the deposition of Cu in oxide film occurs within the Si nodules and under the Cr enriched layer. It was observed in the previous part that the Cu ions could be complexed with the substrate namely Fe-oxide and Cr-oxide and they have higher intensities in the deeper layer. That can be a reason for the observation of Cu in the deeper layer. It can be suggested that the presence of Cu containing components in the deppth is facilitated by F^- ions that can dissolve the oxide film or they can peneterate through the oxide film via the porosity in the oxide layer [4].

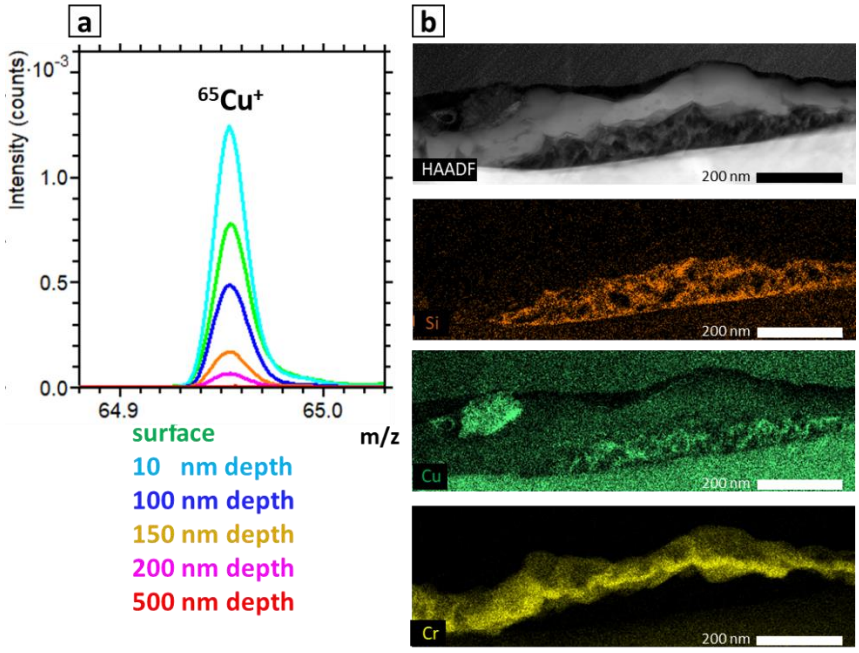

Fig. 9: The ToF-SIMS depth profile of Cu^{+} at the different depths (a) and the HAADF-STEM image of an area of the oxide film and the corresponding Si, Cu, and Cr EDX maps (b)

4.6 Formation mechanism of the coating

As it was reported in the literature, Cu can have a great influence on the distribution of Zr oxide all over the surface and its oxidation state can give insight into the mechanism [15,31,50]. In these cases, like Al and Zn, the thin oxide layer (native oxide) is removed by F ions and that facilitates access to the metal substrate. The further dissolution/oxidation of the metal substrate provides the necessary electrons for the reduction of Cu and its deposition on the surface. The reactions below clarify the abovementioned statement where M is the metal:

$$M \rightarrow M^{n+} + ne^{-}$$

$$Cu^{2+} + 2e^{-} \rightarrow Cu\downarrow$$

In the case of the current substrate, the stainless steel is covered by a thick oxide layer and it was shown before that the full removal of this thermal oxide film is not possible. Instead, the oxide film will dissolve preferentially in the zones that are more soluble in the pickling process such as Fe containing oxide [3,4]. Therefore, there was no clear indication for the contribution of metal in the oxidation reaction. This is why it is necessary to determine the composition of Cu to see if this substrate follows the above reactions or not.

In this study, the results showed that Cu can have 3 different compositions on the surface and in-depth.

1. Cu oxide/hydroxide: Cu^{2+} can be immediately reduced ($Cu^{2+} + e^{-} \rightarrow Cu^{+}$) and be further oxidized in contact with air or solution and form Cu oxide/hydroxide.

2. Cu-AS: this component is in a low concentration present on the outer layer covering some of the Cu oxide /hydroxide particles from the reduction of Cu^{2+}. The amine groups in the aminosilane molecule can be complexed with Cu through an acceptor-donor reaction.
3. Cu-Fe/Cr: The Cu ions can be complexed with the dissolved Fe-oxide and Cr-oxide during pickling reaction and form Cu-Cr/Fe oxide on the surface and in depth.

From the presence of these compounds, the anodic counter reaction can be the dissolution of the substrate where the less stable components can be dissolved into the solution [4,17,19]. This dissolution can happen during the below reaction:

$$FeCr_2O_4 + 3F^- \rightarrow FeF_3 + Cr_2O_4^{2-} + e^-$$

$$FeCr_2O_3 + 2F^- \rightarrow FeF_2 + 2e^- + Cr_2O_3$$

The formation of Fe-F compound and the enrichment of surface by Cr oxide during pickling step have been shown in our previous research [3].

Fig. 10 illustrates the formation of the hybrid Zr-AS coating on our substrate containing a complex thermal oxide film, which chemical structure characterization has been carried out in our previous research [3,4].

Deposition of Cu with different oxidation states leads to a variation of Zr oxide deposition all over the surface. In a conventional Zr-based conversion coating with the addition of Cu, the deposition of Cu oxide or metallic Cu results in the acceleration of Zr oxide deposition due to its higher cathodic activity. In addition, Cu^{2+} consumes the free electrons from anodic reaction which leads to the acceleration of substrate oxidation or dissolution. However, the formation of the Zr oxide happens mainly around Cu particles preventing the formation of a homogenous layer that can impart corrosion protection [15,31].

According to Fig. 10, there are some Cu-oxide/hydroxide particles on the surface along with the presence of higher Zr oxide concentration, showing the promotion of coating deposition around these particles. On the other hand, some of these Cu oxide particles are covered by Cu-AS which does not have the same cathodic activity as Cu-oxide, thus no significant Zr oxide deposition could be observed around them. Eventually, Cu^{2+} could be complexed with the Fe and Cr oxide from the substrate that was observed in the deeper zones.

Furthermore, a very thin layer containing Si and N covers the whole surface which represents the deposition of free aminosilane in the solution. This layer is reported to improve the adhesion of the next organic layer [51].

These results suggest that the addition of an amine-containing organic additive to the Zr-Cu conversion coating can still accelerate the coating deposition but can hinder a part of Cu function through complexation with this component. This can prevent the selective deposition of Zr oxide only on Cu particles and presumably the formation of a heterogeneous layer. It can be speculated that this combination could greatly improve the adhesion of E-coat and organic coating together with its high corrosion protection.

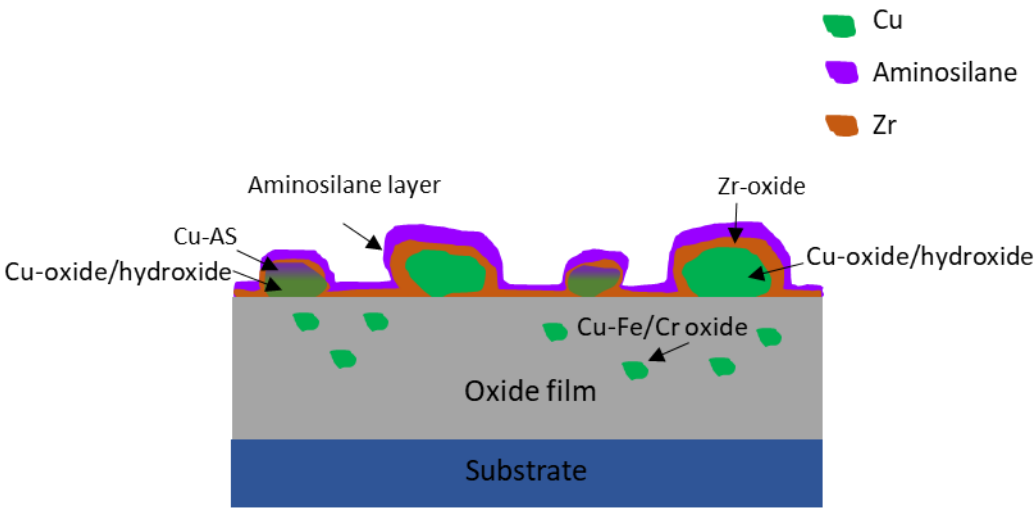

Fig. 10: Schematic illustration of the composition of hybrid Zr-As conversion coating on AHSSS

5 Conclusion

This research aimed to understand the mechanism behind the simultaneous presence of aminosilane and Cu additives in Zr-based conversion treatment. This study was carried out on advanced high strength stainless steel for automotive applications. The results elucidated the below items:

- The treatment of this substrate with the hybrid Zr-AS-Cu conversion coating leads to the formation of Cu-containing particles all over the surface.
- The coating contains an aminosilane layer at the outer surface and Cu and Zr oxides in the lower layer.
- The line profile by FEG-AES showed that the Zr oxide deposition mainly happens around the Cu particles.
- The analysis of the oxidation state of Cu indicated that Cu is present in three different forms, namely Cu-oxide/hydroxide, Cu-As, and Cu-Fe/Cr oxide.
- The presence of both aminosilane and Cu additives leads to the formation of a donor-acceptor complex between amine groups and Cu ions which has less cathodic activity compared to Cu-oxide.
- This interaction can lead to the formation of a more homogenous layer by avoiding the selective deposition of Zr oxide when only Cu is present.

6 Acknowledgment

The authors gratefully acknowledge Sandrine Deprieck from Aperam for performing GDOES measurements and Priya Laha from Vrije Universiteit Brussel for FEG-AES measurement. Moreover, the authors would like to thank Niclas Unger from Chemetall GmbH for his support in the pretreatment process.

7 Data availability

The raw/processed data required to reproduce these findings cannot be shared at this time due to legal or ethical reasons.

8 References

[1] Aperam- Stainless, MaX: Ultra-High Strength Stainless Steel for Lightweight Automotive Applications, Aperam Stainless Steel. (2017). https://www.aperam.com/sites/default/files/documents/2018-05/Aperam_plaquette MaX_0.pdf?template=colorbox (accessed October 19, 2020).

[2] J.B. Moreau, G. Badinier, P.O. Santacreu, B. Petit, J.D. Mithieux, J. Paegle, Lightweight chassis parts made of MaX1.2HY press hardening stainless steel, 6th International Conference Hot Steel Metal Forming of High-Performance Steel, CHS2 2017- Proceedings. (2017) 611–618.

[3] M. Nabizadeh, C. Boissy, K. Baert, S. Goderis, H. Ottevaere, H. Terryn, T. Hauffman, The mechanism of thermal oxide film formation on low Cr martensitic stainless steel and its behavior in fluoride-based pickling solution in conversion treatment, Corrosion Science. 181 (2020) 109206. https://doi.org/10.1016/j.corsci.2020.109206.

[4] M. Nabizadeh, E.A. Mernissi Cherigui, K. Marcoen, T. Kolberg, D. Schatz, A.J. Cruz, R. Ameloot, H. Terryn, T. Hauffman, Unraveling the mechanism of the conversion treatment on Advanced High Strength Stainless Steels (AHSSS), Applied Surface Science. 572 (2022) 151418. https://doi.org/10.1016/J.APSUSC.2021.151418.

[5] G. Badinier, J.B. Moreau, B. Petit, C. Boissy, J.D. Mithieux, S. Saedlou, J. Paegle, Development of press hardening stainless steels for body-in-white application, 6th International Conference Hot Steel Metal Forming of High-Performance Steel. (2017) 77–84.

[6] P.G. Sheasby, S. Wernick, R. Pinner, Surface treatment and finishing of aluminum and its alloys, ASM International/Finishing Publications, 1987.

[7] N. Akafuah, S. Poozesh, A. Salaimeh, G. Patrick, K. Lawler, K. Saito, Evolution of the Automotive Body Coating Process—A Review, Coatings. 6 (2016) 24. https://doi.org/10.3390/coatings6020024.

[8] A.E. Hughes, Conversion coatings, in: Encyclopedia of Interfacial Chemistry: Surface Science and Electrochemistry, Elsevier, 2018: pp. 108–114. https://doi.org/10.1016/B978-0-12-409547-2.13441-9.

[9] M. Doerre, L. Hibbitts, G. Patrick, N. Akafuah, Advances in Automotive Conversion Coatings during Pretreatment of the Body Structure: A Review, Coatings. 8 (2018) 405. https://doi.org/10.3390/coatings8110405.

[10] G. Šekularac, J. Kovač, I. Milošev, Prolonged protection, by zirconium conversion coatings, of AlSi7Mg0.3 aluminium alloy in chloride solution, Corrosion Science. 169 (2020) 108615. https://doi.org/10.1016/J.CORSCI.2020.108615.

[11] D.G. Shchukin, M. Zheludkevich, K. Yasakau, S. Lamaka, M.G.S. Ferreira, H. Möhwald, Layer-by-Layer Assembled Nanocontainers for Self-Healing Corrosion Protection, Advanced Materials. 18 (2006) 1672–1678. https://doi.org/10.1002/ADMA.200502053.

[12] H.J. Streitberger, K.F. Dössel, Automotive Paints and Coatings: Second Edition, John Wiley & Sons, Ltd, Weinheim, Germany, 2008. https://doi.org/10.1002/9783527622375.

[13] H. Ardelean, I. Frateur, P. Marcus, Corrosion protection of magnesium alloys by cerium, zirconium and niobium-based conversion coatings, Corrosion Science. 50 (2008) 1907–1918. https://doi.org/10.1016/J.CORSCI.2008.03.015.

[14] W. Zhou, D. Shan, E.H. Han, W. Ke, Structure and formation mechanism of phosphate conversion coating on die-cast AZ91D magnesium alloy, Corrosion Science. 50 (2008) 329–337. https://doi.org/10.1016/j.corsci.2007.08.007.

[15] S. Adhikari, K.A. Unocic, Y. Zhai, G.S. Frankel, J. Zimmerman, W. Fristad, Hexafluorozirconic acid based surface pretreatments: Characterization and performance assessment, in: Electrochimica Acta, Pergamon, 2011: pp. 1912–1924. https://doi.org/10.1016/j.electacta.2010.07.037.

[16] M. Nabizadeh, A.A. Sarabi, H. Eivaz Mohammadloo, Comparative investigation of Cu ion and adipic acid addition on electrochemical and microstructure characteristics of vanadium conversion coating on AZ31 Mg alloy, Surface and Coatings Technology. 357 (2019) 1–11. https://doi.org/10.1016/j.surfcoat.2018.10.012.

[17] P. Taheri, P. Laha, H. Terryn, J.M.C. Mol, An in situ study of zirconium-based conversion treatment on zinc surfaces, Applied Surface Science. 356 (2015) 837–843. https://doi.org/10.1016/j.apsusc.2015.08.205.

[18] F.O. George, P. Skeldon, G.E. Thompson, Formation of zirconium-based conversion coatings on aluminium and Al-Cu alloys, Corrosion Science. 65 (2012) 231–237. https://doi.org/10.1016/j.corsci.2012.08.031.

[19] P. Taheri, K. Lill, J.H.W. de Wit, J.M.C. Mol, H. Terryn, Effects of Zinc Surface Acid-Based Properties on Formation Mechanisms and Interfacial Bonding Properties of Zirconium-Based Conversion Layers, (2012). https://doi.org/10.1021/jp209422d.

[20] L.I. Fockaert, P. Taheri, S.T. Abrahami, B. Boelen, H. Terryn, J.M.C. Mol, Zirconium-based conversion film formation on zinc, aluminium and magnesium oxides and their interactions with functionalized molecules, Applied Surface Science. 423 (2017) 817–828. https://doi.org/10.1016/j.apsusc.2017.06.174.

[21] L.I. Fockaert, S. Pletincx, B. Boelen, T. Hauffman, H. Terryn, J.M.C. Mol, Effect of zirconium-based conversion treatments of zinc, aluminium and magnesium on the chemisorption of ester-functionalized molecules, Applied Surface Science. 508 (2020). https://doi.org/10.1016/j.apsusc.2019.145199.

[22] J.H. Nordlien, J.C. Walmsley, H. Østerberg, K. Nisancioglu, Formation of a zirconium-titanium based conversion layer on AA 6060 aluminium, Surface and Coatings Technology. 153 (2002) 72–78. https://doi.org/10.1016/S0257-8972(01)01663-2.

[23] O. Lunder, C. Simensen, Y. Yu, K. Nisancioglu, Formation and characterisation of Ti–Zr based conversion layers on AA6060 aluminium, Surface and Coatings Technology. 184 (2004) 278–290. https://doi.org/10.1016/J.SURFCOAT.2003.11.003.

[24] H. Eivaz Mohammadloo, A.A. Sarabi, A.A. Sabbagh Alvani, H. Sameie, R. Salimi, Nano-ceramic hexafluorozirconic acid based conversion thin film: Surface characterization and electrochemical study, Surface and Coatings Technology. 206 (2012) 4132–4139. https://doi.org/10.1016/J.SURFCOAT.2012.04.009.

[25] V. Cristaudo, K. Baert, P. Laha, M. Lyn Lim, E. Brown-Tseng, H. Terryn, T. Hauffman, A combined XPS/ToF-SIMS approach for the 3D compositional characterization of Zr-based conversion of galvanized steel, Applied Surface Science. 562 (2021) 150166. https://doi.org/10.1016/J.APSUSC.2021.150166.

[26] S. Verdier, N. van der Laak, F. Dalard, J. Metson, S. Delalande, An electrochemical and SEM study of the mechanism of formation, morphology, and composition of titanium or zirconium fluoride-based coatings, Surface and Coatings Technology. 200 (2006) 2955–2964. https://doi.org/10.1016/J.SURFCOAT.2004.10.139.

[27] F. Andreatta, A. Turco, I. de Graeve, H. Terryn, J.H.W. de Wit, L. Fedrizzi, SKPFM and SEM study of the deposition mechanism of Zr/Ti based pre-treatment on AA6016 aluminum alloy, Surface and Coatings Technology. 201 (2007) 7668–7685. https://doi.org/10.1016/J.SURFCOAT.2007.02.039.

[28] A. Sarfraz, R. Posner, M.M. Lange, K. Lill, A. Erbe, Role of Intermetallics and Copper in the Deposition of ZrO2 Conversion Coatings on AA6014, Journal of The Electrochemical Society. 161 (2014) C509. https://doi.org/10.1149/2.0121412JES.

[29] H. Eivaz Mohammadloo, A.A. Sarabi, R. Mohammad Hosseini, M. Sarayloo, H. Sameie, R. Salimi, A comprehensive study of the green hexafluorozirconic acid-based conversion coating, Progress in Organic Coatings. 77 (2014) 322–330. https://doi.org/10.1016/J.PORGCOAT.2013.10.006.

[30] R. Mohammad Hosseini, A.A. Sarabi, H. Eivaz Mohammadloo, M. Sarayloo, The performance improvement of Zr conversion coating through Mn incorporation: With and without organic coating, Surface and Coatings Technology. 258 (2014) 437–446. https://doi.org/10.1016/J.SURFCOAT.2014.08.056.

[31] T. Lostak, S. Krebs, A. Maljusch, T. Gothe, M. Giza, M. Kimpel, J. Flock, S. Schulz, Formation and characterization of Fe3+-/Cu2+-modified zirconium oxide conversion layers on zinc alloy coated steel sheets, Electrochimica Acta. 112 (2013) 14–23. https://doi.org/10.1016/j.electacta.2013.08.161.

[32] L. Li, B.W. Whitman, G.M. Swain, Characterization and Performance of a Zr/Ti Pretreatment Conversion Coating on AA2024-T3, Journal of The Electrochemical Society. 162 (2015) C279. https://doi.org/10.1149/2.0901506JES.

[33] J. Cerezo, I. Vandendael, R. Posner, K. Lill, J.H.W. de Wit, J.M.C. Mol, H. Terryn, Initiation and growth of modified Zr-based conversion coatings on multi-metal surfaces, Surface and Coatings Technology. 236 (2013) 284–289. https://doi.org/10.1016/j.surfcoat.2013.09.059.

[34] Q. Meng, G.S. Frankel, Effect of copper content on chromate conversion coating protection of 7xxx-T6 aluminum alloys, Corrosion. 60 (2004) 897–905. https://doi.org/10.5006/1.3287823.

[35] P. Campestrini, H. Terryn, A. Hovestad, J.H.W. de Wit, Formation of a cerium-based conversion coating on AA2024: Relationship with the microstructure, Surface and Coatings Technology. 176 (2004) 365–381. https://doi.org/10.1016/S0257-8972(03)00743-6.

[36] X. Liu, D. Vonk, H. Jiang, K. Kisslinger, X. Tong, M. Ge, E. Nazaretski, B. Ravel, K. Foster, S. Petrash, Y.C.K. Chen-Wiegart, Environmentally Friendly Zr-Based Conversion Nanocoatings for Corrosion Inhibition of Metal Surfaces Evaluated by Multimodal X-ray Analysis, ACS Applied Nano Materials. 2 (2019) 1920–1929. https://doi.org/10.1021/acsanm.8b02309.

[37] P. Campestrini, G. Goeminne, H. Terryn, J. Vereecken, J.H.W. de Wit, Chromate conversion coating on aluminum alloys I. formation mechanism, J Electrochem Soc. 151 (2004). https://doi.org/10.1149/1.1637355.

[38] A.E. Hughes, J.D. Gorman, P.J.K. Paterson, The characterisation of Ce-Mo-based conversion coatings on Al-alloys: Part I, Corrosion Science. 38 (1996) 1957–1976. https://doi.org/10.1016/S0010-938X(96)00088-1.

[39] J. Cerezo, I. Vandendael, R. Posner, J.H.W. de Wit, J.M.C. Mol, H. Terryn, The effect of surface pre-conditioning treatments on the local composition of Zr-based conversion coatings formed on aluminium alloys, Applied Surface Science. 366 (2016) 339–347. https://doi.org/10.1016/j.apsusc.2016.01.106.

[40] I. de Graeve, J. Vereecken, A. Franquet, T. van Schaftinghen, H. Terryn, Silane coating of metal substrates: Complementary use of electrochemical, optical and thermal analysis for the evaluation of film properties, Progress in Organic Coatings. 59 (2007) 224–229. https://doi.org/10.1016/j.porgcoat.2006.09.006.

[41] I. de Graeve, E. Tourwé, M. Biesemans, R. Willem, H. Terryn, Silane solution stability and film morphology of water-based bis-1,2-(triethoxysilyl)ethane for thin-film deposition on aluminium, Progress in Organic Coatings. 63 (2008) 38–42. https://doi.org/10.1016/j.porgcoat.2008.04.002.

[42] A. Franquet, H. Terryn, J. Vereecken, IRSE study on effect of thermal curing on the chemistry and thickness of organosilane films coated on aluminium, Applied Surface Science. 211 (2003) 259–269. https://doi.org/10.1016/S0169-4332(03)00258-7.

[43] T. van Schaftinghen, C. le Pen, H. Terryn, F. Hörzenberger, Investigation of the barrier properties of silanes on cold rolled steel, in: Electrochimica Acta, Pergamon, 2004: pp. 2997–3004. https://doi.org/10.1016/j.electacta.2004.01.059.

[44] S. Akhtar, A. Matin, A. Madhan Kumar, A. Ibrahim, T. Laoui, Enhancement of anticorrosion property of 304 stainless steel using silane coatings, Applied Surface Science. 440 (2018) 1286–1297. https://doi.org/10.1016/j.apsusc.2018.01.203.

[45] R. Moore, B. Dunham, Zirconization™: The future of coating pretreatment processes: Alternative, phosphate-free, eco-friendly pretreatment procedure addresses energy and chemical consumption while improving product quality., Metal Finishing. 106 (2008) 46–55. https://doi.org/10.1016/S0026-0576(08)80259-0.

[46] W. Yuan, W.J. van Ooij, Characterization of Organofunctional Silane Films on Zinc Substrates, Journal of Colloid and Interface Science. 185 (1997) 197–209. https://doi.org/10.1006/JCIS.1996.4604.

[47] D.R. Vonk, I.T.S. Smith, A. Bobadilla, Thin corrosion protective coatings incorporating polyamidoamine polymers, US Patent 20180037770. (2017).

[48] I. Milošev, G.S. Frankel, Review—Conversion Coatings Based on Zirconium and/or Titanium, Journal of The Electrochemical Society. 165 (2018). https://iopscience.iop.org/article/10.1149/2.0371803jes.

[49] B. Ramezanzadeh, H. Vakili, R. Amini, The effects of addition of poly(vinyl) alcohol (PVA) as a green corrosion inhibitor to the phosphate conversion coating on the anticorrosion and adhesion properties of the epoxy coating on the steel substrate, Applied Surface Science. 327 (2015) 174–181. https://doi.org/10.1016/j.apsusc.2014.11.167.

[50] X. Liu, D. Vonk, K. Kisslinger, X. Tong, G. Halada, S. Petrash, K. Foster, Y.C.K. Chen-Wiegart, Unraveling the Formation Mechanism of a Hybrid Zr-Based Chemical Conversion Coating with Organic and Copper Compounds for Corrosion Inhibition, ACS Applied Materials and Interfaces. 13 (2021) 5518–5528. https://doi.org/10.1021/acsami.0c19203.

[51] T. Lostak, C. Timma, S. Krebs, J. Flock, S. Schulz, Organosilane modified Zr-based conversion layer on Zn–Al alloy coated steel sheets, Surface and Coatings Technology. 305 (2016) 223–230. https://doi.org/10.1016/j.surfcoat.2016.08.030.

[52] M.C. Biesinger, Advanced analysis of copper X-ray photoelectron spectra, Surface and Interface Analysis. 49 (2017) 1325–1334. https://doi.org/10.1002/sia.6239.

[53] M.C. Biesinger, L.W.M. Lau, A.R. Gerson, R.S.C. Smart, Resolving surface chemical states in XPS analysis of first row transition metals, oxides and hydroxides: Sc, Ti, V, Cu and Zn, Applied Surface Science. 257 (2010) 887–898. https://doi.org/10.1016/j.apsusc.2010.07.086.

[54] Y. van Ingelgem, I. Vandendael, J. Vereecken, A. Hubin, Study of copper corrosion products formed during localized corrosion using field emission Auger electron spectroscopy, Surface and Interface Analysis. 40 (2008) 273–276. https://doi.org/10.1002/SIA.2744.

[55] L. Wu, H. Wang, H. Lan, H. Liu, J. Qu, Adsorption of Cu(II)–EDTA chelates on tri-ammonium-functionalized mesoporous silica from aqueous solution, Separation and Purification Technology. 117 (2013) 118–123. https://doi.org/10.1016/J.SEPPUR.2013.06.016.

[56] M.R. Kotte, A.T. Kuvarega, M. Cho, B.B. Mamba, M.S. Diallo, Mixed Matrix PVDF Membranes With in Situ Synthesized PAMAM Dendrimer-Like Particles: A New Class of Sorbents for Cu(II) Recovery from Aqueous Solutions by Ultrafiltration, Environmental Science and Technology. 49

(2015) 9431–9442. https://doi.org/10.1021/ACS.EST.5B01594/SUPPL_FILE/ES5B01594_SI_001.PDF.

[57] J. Kang, H. Liu, Y.M. Zheng, J. Qu, J.P. Chen, Systematic study of synergistic and antagonistic effects on adsorption of tetracycline and copper onto a chitosan, Journal of Colloid and Interface Science. 344 (2010) 117–125. https://doi.org/10.1016/J.JCIS.2009.11.049.

[58] J.C.S. Terra, A. Moores, F.C.C. Moura, Amine-Functionalized Mesoporous Silica as a Support for on-Demand Release of Copper in the A3-Coupling Reaction: Ultralow Concentration Catalysis and Confinement Effect, ACS Sustainable Chemistry & Engineering. 7 (2019) 8696–8705. https://doi.org/10.1021/ACSSUSCHEMENG.9B00576.

[59] M.S. Diallo, S. Christie, P. Swaminathan, L. Balogh, X. Shi, W. Um, C. Papelis, W.A.G. Iii, J.H. Johnson, Dendritic Chelating Agents. 1. Cu(II) Binding to Ethylene Diamine Core Poly(amidoamine) Dendrimers in Aqueous Solutions, (2004). https://doi.org/10.1021/la036108k.

[60] *†,‡ Mamadou S. Diallo, § Lajos Balogh, ⊥ Abdul Shafagati, Jr.,⊥ James H. Johnson, I. and William A. Goddard, ‖ Donald A. Tomalia§, Poly(amidoamine) Dendrimers: A New Class of High Capacity Chelating Agents for Cu(II) Ions, Environmental Science and Technology. 33 (1999) 820–824. https://doi.org/10.1021/ES980521A.

[61] W. Maketon, C.Z. Zenner, K.L. Ogden, Removal Efficiency and Binding Mechanisms of Copper and Copper−EDTA Complexes Using Polyethyleneimine, Environmental Science and Technology. 42 (2008) 2124–2129. https://doi.org/10.1021/ES702420H.

[62] D. Kowalczyk, S. Slomkowski, M.M. Chehimi, M. Delamar, Adsorption of aminopropyltriethoxy silane on quartz: an XPS and contact angle measurements study, International Journal of Adhesion and Adhesives. 16 (1996) 227–232. https://doi.org/10.1016/0143-7496(95)00052-6.

[63] R.F. Comrie, S.M. MacDonald, Interaction of a model epoxy resin compound, diethanolamine, with aluminium surfaces studied by static SIMS and XPS, J. Chem. Soc., Faraday T Rans. 94 (1998).

[64] R.A. Shircliff, P. Stradins, H. Moutinho, J. Fennell, M.L. Ghirardi, S.W. Cowley, H.M. Branz, I.T. Martin, Angle-Resolved XPS Analysis and Characterization of Monolayer and Multilayer Silane Films for DNA Coupling to Silica, Langmuir. 29 (2013) 4057–4067. https://doi.org/10.1021/LA304719Y.

[65] S.T. Abrahami, T. Hauffman, J.M.M. de Kok, J.M.C. Mol, H. Terryn, XPS Analysis of the Surface Chemistry and Interfacial Bonding of Barrier-Type Cr(VI)-Free Anodic Oxides, (2015). https://doi.org/10.1021/acs.jpcc.5b05958.

[66] A.A. Fiorillo, J.M. Galbraith, A Valence Bond Description of Coordinate Covalent Bonding†, Journal of Physical Chemistry A. 108 (2004) 5126–5130. https://doi.org/10.1021/JP049632O.

[67] A.Y. Timoshkin, G. Frenking, Low-Valent Group-13 Chemistry. Theoretical Investigation of the Structures and Relative Stabilities of Donor−Acceptor Complexes R3E−E‘R‘ and Their Isomers R2E−E‘RR‘ †, J Am Chem Soc. 124 (2002) 7240–7248. https://doi.org/10.1021/JA0201754.

[68] K. Marcoen, M. Gauvin, J. de Strycker, H. Terryn, T. Hauffman, Molecular Characterization of Multiple Bonding Interactions at the Steel Oxide–Aminopropyl triethoxysilane Interface by ToF-SIMS, ACS Omega. 5 (2020) 692–700. https://doi.org/10.1021/ACSOMEGA.9B03330.